Astronomy & Astrophysics manuscript no. paper
April 26, 2006

A PDR-Code comparison study

M. Röllig[1], N. P. Abel[2], T. Bell[3], F. Bensch[4], J. Black[15], G. J. Ferland[2], B. Jonkheid[5], I. Kamp[6], M.J. Kaufman[7], J. Le Bourlot[8], F. Le Petit[8,15], R. Meijerink[5], O. Morata Chirivella[16], V. Ossenkopf[1,10], E. Roueff[8], G. Shaw[2], M. Spaans[9], A. Sternberg[11], J. Stutzki[1], W.-F. Thi[12], E. F. van Dishoeck[5], P. A. M. van Hoof[13], S. Viti[3], M.G. Wolfire[14]

[1] I. Physikalisches Institut, Universität zu Köln, Zülpicher Str. 77, D-50937 Köln, Germany,
[2] University of Kentucky, Department of Physics and Astronomy, Lexington, KY 40506,
[3] Department of Physics & Astronomy, University College London, Gower Street, London WC1E 6BT,
[4] Argelander-Institut für Astronomie ⋆, Universität Bonn, Auf dem Hügel 71, D-53121 Bonn, Germany,
[5] Leiden Observatory, P.O. Box 9513, NL-2300 RA Leiden, Netherlands,
[6] Space Telescope Science Division of ESA, Space Telescope Science Institute, Baltimore, MD 21218,
[7] Department of Physics, San Jose State University, 1 Washington Square, San Jose, CA 95192,
[8] LUTH UMR 8102, CNRS and Observatoire de Paris, Place J. Janssen 92195 Meudon Cedex, France,
[9] Kapteyn Astronomical Institute, PO Box 800, 9700 AV Groningen, The Netherlands,
[10] SRON Netherland Institute for Space Research, Postbus 800, 9700 AV Groningen, Netherlands,
[11] School of Physics and Astronomy, Tel Aviv University, Ramat Aviv 69978, Israel,
[12] Sterrenkundig Instituut Anton Pannekoek, University of Amsterdam, Kruislaan 403 1098 SJ Amsterdam, The Netherlands,
[13] Royal Observatory of Belgium, Av. Circulaire, 3 - Ringlaan 3,1180 BRUXELLES - BRUSSEL
[14] Astronomy Department, University of Maryland, College Park, MD 20742-2421
[15] Onsala Space Observatory, 439 92 Onsala, Sweden
[16] LAEFF, Villafranca del Castillo, Apdo. 50727, E-28080 Madrid, Spain

Preprint online version: April 26, 2006

ABSTRACT

Aims. We present a comparison between independent computer codes, modeling the physics and chemistry of photon dominated regions (PDRs). Our goal was to understand the mutual differences in the PDR codes and their effects on the physical and chemical structure of the model clouds, and to converge the output of different codes to a common solution.
Methods. A number of benchmark models have been calculated, covering low and high gas densities $n = 10^3, 10^{5.5}$ cm^{-3} and far ultraviolet intensities $\chi = 10, 10^5$ (FUV: $6 < h\nu < 13.6$ eV). The benchmark models were computed in two ways: one set assuming constant temperatures, thus testing the consistency of the chemical network and photo-reactions, and a second set determining the temperature self consistently by solving the thermal balance, thus testing the modeling of the heating and cooling mechanisms accounting for the detailed energy balance throughout the clouds.
Results. We investigated the impact of PDR geometry and agreed on the comparison of results from spherical and plane-parallel PDR models. We identified a number of key processes governing the chemical network which have been treated differently in the various codes such as the effect of PAHs on the electron density or the temperature dependence of the dissociation of CO by cosmic ray induced secondary photons, and defined a proper common treatment. We established a comprehensive set of reference models for ongoing and future PDR modeling and were able to increase the agreement in model predictions for all benchmark models significantly. Nevertheless, the remaining spread in the computed observables such as the atomic fine-structure line intensities serves as a warning that the astronomical data should not be overinterpreted.

Key words. ISM: abundances – Astrochemistry – ISM: clouds – ISM: general – Radiative Transfer – Methods: numerical

1. Introduction

Photon dominated regions or photodissociation regions (PDRs) play an important role in modern astrophysics as they are responsible for many emission characteristics of the ISM, and dominate the infrared and submillimetre spectra of star formation regions and galaxies as a whole. Theoretical models addressing the structure of PDRs have been available for approximately 30 years and have evolved into advanced computer codes accounting for a growing number of physical effects with increasing accuracy. These codes have been developed with

Send offprint requests to: M. Röllig,
e-mail: roellig@ph1.uni-koeln.de
⋆ Founded by merging of the Sternwarte, Radiastronomisches Institut and Institut für Astrophysik und Extraterestrische Forschung

different goals in mind: some are geared to efficiently model a particular type of region, e.g. HII regions, protoplanetary disks, planetary nebulae, diffuse clouds, etc.; others emphasize a strict handling of the micro-physical processes in full detail (e.g. wavelength dependent absorption), but at the cost of increased computing time. Yet others aim at efficient and rapid calculation of large model grids for comparison with observational data, which comes at the cost of pragmatic approximations using effective rates rather than detailed treatment. As a result, the different models have focused on the detailed simulation of different processes determining the structure in the different regions while using only rough approximations for other processes. The model setups vary greatly among different model codes. This includes the assumed model geometry, their physical and chemical structure, the choice of free parameters, and other details. Consequently it is not always straightforward to directly compare the results from different PDR codes. Taking into account that there are multiple ways of implementing physical effects in numerical codes, it is obvious that the model output of different PDR codes can differ from each other. As a result, significant variations in the physical and chemical PDR structure predicted by the various PDR codes can occur. This divergency would prevent a unique interpretation of observed data in terms of the parameters of the observed clouds. Several new facilities such as Herschel, SOFIA, APEX, ALMA, and others will become available over the next years and will deliver many high quality observations of line and dust continuum emission in the sub-millimeter and FIR wavelength regime. Many important PDR tracers emit in this range ([CII] (158μm), [OI] (63 and 146 μm), [CI] (370 and 610 μm), CO (650, 520, ..., 57.8 μm), H_2O, etc.). In order to reliably analyze these high quality data we need a set of high quality tools, including PDR models that are well understood and properly debugged. As an important preparatory step toward these missions an international cooperation between many PDR model groups was initialized. The goals of this PDR-benchmarking were:

- to understand the differences in the different code results
- to obtain (as much as possible) the same model output with every PDR code when using the same input
- to agree on the correct handling of important processes
- to identify the specific limits of applicability of the available codes

To this end, a PDR-benchmarking workshop was held at the Lorentz Center in Leiden, Netherlands in 2004 to jointly work on these topics (URL: `http://www.lorentzcenter.nl/`). In this paper we present the results from this workshop and the results originating from the follow-up activities. A related workshop to test line radiative transfer codes was held in 1999 (see van Zadelhoff et al., 2002, for results).

It is not the purpose of the benchmarking to present a preferred solution or a preferred code. PDRs are found in a large variety of objects and under very different conditions. To this end, it was neither possible nor desirable to develop a *generic* PDR code, able to model every possible PDR. Every participating code was developed for a particular field of application, and has its individual strengths and weaknesses. Furthermore, the benchmarking is not meant to model any 'real' astronomical object. The main purpose of this study is technical not physical. This is also reflected in the choice of the adopted incomplete chemical reaction network (see § 4).

In § 2 we briefly introduce the physics involved in PDRs, in § 3 we introduce some key features in PDR modeling. § 4 describes the setup of the benchmark calculations and § 5 presents the results for a selection of benchmark calculations and gives a short review over the participating codes. In § 6 we discuss the results and summarize the lessons, learned from the benchmark effort. A tabular overview of the individual code characteristics is given in the Appendix.

2. The Physics of PDRs

It is common to distinguish between HII regions and PDRs, even if it is unquestioned that HII regions are also dominated by photons. The transition from HII region to PDR takes place when FUV photons with energies larger than the ionization energy of hydrogen (13.6 eV) are efficiently used up[1]. In PDRs the gas is heated by the far-ultraviolet radiation (FUV, $6 < h\nu < 13.6$ eV, from the ambient UV field and from hot stars) and cooled via the emission of spectral line radiation of atomic and molecular species and continuum emission by dust (Hollenbach & Tielens 1999, Sternberg 2004). The FUV photons are heating the gas by means of photoelectric emission from grain surfaces and polycyclic aromatic hydrocarbons (PAHs) and by collisional de-excitation of vibrationally excited H_2 molecules. Additional contribution to the total gas heating comes from H_2 formation, dissociation of H_2, dust-gas collisions in case of dust temperatures exceeding the gas temperature, cosmic ray heating, turbulence heating, and from chemical heating. At low visual extinction A_V the gas is cooled by emission of atomic fine-structure lines, mainly [CII] 158μm and [OI] 63μm. At larger depths, millimeter, sub-millimeter and far-infrared molecular rotational-line cooling (CO, OH, H_2, H_2O) becomes important, and a correct treatment of the radiative transfer in the line cooling is critical. The balance between heating and cooling determines the local gas temperature. The local FUV intensity also influences the chemical structure, i.e. the abundance of the individual chemical constituents of the gas. The surface of PDRs is mainly dominated by reactions induced by UV photons, especially the ionization and dissociation of atoms and molecules. With diminishing mean FUV intensity at higher optical depths more complex species may be formed without being radiatively destroyed immediately. Thus the overall structure of a PDR is the result of a very complex interplay between radiative transfer, energy balance, and chemical reactions.

3. Modeling of PDRs

The history of PDR modeling started in the early 1970's (Hollenbach et al., 1971; Jura, 1974; Glassgold & Langer,

[1] This distinction is clearer when referring to PDRs as Photo-Dissociation Regions, since dissociable molecules are hardly found in HII regions

1975; Black & Dalgarno, 1977) with steady state models for the transitions from H to H_2 and from C^+ to CO. In the following years a number of models, addressing the chemical and thermal structure of clouds subject to an incident flux of FUV photons have been developed (de Jong et al., 1980; Tielens & Hollenbach, 1985; van Dishoeck & Black, 1988; Sternberg & Dalgarno, 1989; Hollenbach et al., 1991; Le Bourlot et al., 1993; Störzer et al., 1996). Additionally, a number of models, focusing on certain aspects of PDR physics and chemistry were developed, e.g. models accounting for time-dependent chemical networks, models of clumped media, and turbulent PDR models (Wagenblast & Hartquist, 1988; de Boisanger et al., 1992; Lee et al., 1996; Hegmann & Kegel, 1996; Spaans, 1996; Nejad & Wagenblast, 1999; Röllig et al., 2002; Papadopoulos et al., 2002). Standard PDR models generally do not account for dynamical properties of gas. For a more detailed review see Hollenbach & Tielens (1999).

In order to numerically model a PDR it is necessary to compute all local properties of a cloud such as the relative abundances of the gas constituents together with their level populations, temperature of gas and dust, gas pressure, composition of dust/PAHs, and many more. This local treatment is complicated by the radiation field which couples remote parts of the cloud. The local mean radiation field, which is responsible for photochemical reactions, gas/dust heating, and excitation of molecules heavily depends on the position inside the cloud and the (wavelength dependent) absorption along the lines of sight toward this position. This non-local coupling makes numerical PDR calculations a CPU time consuming task.

PDR modelers and observers approach the PDRs from opposite sides: PDR models start by calculating the local properties of the clouds like the local CO density and the corresponding gas temperature and use these local properties to infer the expected global properties of the cloud like total emergent emissivities or fluxes and column densities. The observer on the other hand starts by observing global features of a source and tries to infer the local properties from that. The connection between local and global properties is complex and not necessarily unambiguous. Large uncertainties in e.g. the CO density at the surface of the cloud may result in a relatively unaffected value for the CO column density due to the dominance of the high central density. If one is interested in the total column density it does not matter if different codes produce a different surface CO density. For the interpretation of high-J CO emission lines, however different CO densities in the outer cloud layers make a difference since high temperatures are required to produce sufficiently high-J CO fluxes, and different PDR codes can lead to different interpretations. Thus, if different PDR model codes deviate in their predicted cloud structures, this may impact the interpretation of observations and may prevent inference of the 'true' structure behind the observed data. To this end it is very important to understand the origin of present differences in PDR model calculations. Otherwise it is impossible to rule out alternative interpretations. The ideal situation, from the modelers point of view, would be a complete knowledge of the true local structure of a real cloud **and** their global observable properties. This would easily allow us to calibrate PDR models. Since this case is unobtainable, we take one step back and apply a different approach: If all PDR model codes use the exact same input and the same model assumptions they should theoretically produce the same predictions.

Because of the close interaction between chemical and thermal balance and radiative transfer, PDR codes typically iterate through the following computation steps: 1) solve the local chemical balance to determine local densities, 2) solve the local energy balance to estimate the local physical properties like temperatures, pressures, and level populations, 3) solve the radiative transfer, 4) depending on the geometrical setup (for example semi-infinite slab vs. finite slab) it may be necessary to successively iterate steps 1)-3). Each step requires a variety of assumptions and simplifications. Each of these aspects can be investigated to great detail and complexity (see for example van Zadelhoff et al. (2002) for a discussion of NLTE radiative transfer methods), but the explicit aim of the PDR comparison workshop was to understand the interaction of all computation steps mentioned above. Even so it was necessary to considerably reduce the model complexity in order to disentangle cause and effect.

3.1. Description of Sensitivities and Pitfalls

Several aspects of PDR modeling have shown the need for detailed discussion, easily resulting in misleading conclusions if not treated properly:

3.1.1. Model Geometry

The most important quantity describing the radiation field in PDR models is the local mean intensity (or alternatively the energy density) as given by:

$$J_\nu = \frac{1}{4\pi}\int I_\nu \, d\Omega \quad [\mathrm{erg\ cm^{-2}\ s^{-1}\ Hz^{-1}\ sr^{-1}}] \tag{1}$$

with the specific intensity I_ν being averaged over the solid angle Ω. Note that when referring to the ambient FUV in units of Draine χ (Draine, 1978) or Habing G_0 (Habing, 1968) fields, these are always given as averaged over 4π. If we place a model cloud of sufficient optical thickness, like implicated by a semi-infinite cloud, in such an average FUV field, the resulting local mean intensity at the cloud edge is half the value of that without the cloud. The choice between directed and isotropic FUV fields directly influences the attenuation due to dust. In the uni-directional case the FUV intensity along the line of sight is attenuated according to $\exp(-\tau)$, where τ is the optical depth of the dust. For pure absorption, and accounting for non-perpendicular lines of sight the radiative transfer equation becomes:

$$\mu \frac{dI_\nu(\mu, x)}{dx} = -\kappa_\nu I_\nu(\mu, x) \quad . \tag{2}$$

with the cosine of direction $\mu = \cos\Theta$, the cloud depth x, and the absorption coefficient κ_ν. For the isotropic case, $I_0(\mu) = J_0 = const.$, integration of Eq. 2 leads to the second order exponential integral:

$$J/J_0 = E_2(\tau) = \int_0^1 \frac{\exp(-\tau\mu)}{\mu^2}\, d\mu \tag{3}$$

The attenuation with depth in the isotropic case is significantly different from the uni-directional case. A common way to describe the depth dependence of a particular quantity in PDRs is to plot it against A_V, which is a direct measure of the traversed column of attenuating material. In order to compare the uni-directional and the isotropic case it is necessary to rescale them to the same axis. It is possible to define an effective $A_{V,\mathrm{eff}} = -\ln[E_2(A_V)]$ in the isotropic case, where A_V is the attenuation perpendicular to the surface, i.e. the smallest column of material to the surface. In this paper all results from spherical models are scaled to $A_{V,\mathrm{eff}}$.

3.1.2. Chemistry

PDR chemistry has been addressed in detail by many authors (Tielens & Hollenbach, 1985; van Dishoeck & Black, 1988; Hollenbach et al., 1991; Fuente et al., 1993; Le Bourlot et al., 1993; Jansen et al., 1995; Sternberg & Dalgarno, 1995; Lee et al., 1996; Bakes & Tielens, 1998; Walmsley et al., 1999; Savage & Ziurys, 2004; Teyssier et al., 2004; Fuente et al., 2005; Meijerink & Spaans, 2005). These authors discuss numerous aspects of PDR chemistry in great detail and give a comprehensive overview of the field. At this point we repeat some crucial points in the chemistry of PDRs in order to motivate the benchmark standardization and to prepare the discussion of the benchmark result.

Chemistry in PDRs differs from standard, interstellar chemistry. Photoprocesses are very important due to the high FUV intensity, as well as reactions with atomic H. Of major importance for the chemistry in PDRs, and heavily influenced by the FUV field is the formation and destruction of H_2. H_2 forms on grain surfaces, a process which crucially depends on the temperatures of the gas and the grains (Hollenbach & Salpeter, 1971; Cazaux & Tielens, 2004), which themselves depend on the local cooling and heating, governed by the FUV. The photodissociation of H_2 is a line absorption process and, thus is subject to effective shielding (van Dishoeck & Black, 1988). This leads to a rapid transformation from atomic to molecular hydrogen once the H_2 absorption lines are optically thick. The photo-dissociation of CO is also a line absorption process, additionally complicated by the fact that the broad H_2 absorption lines overlap with CO absorption lines. Similar to H_2 this leads to a transition from atomic carbon to CO. For $A_V < 1$ carbon is predominantly present in ionized form. CO is formed at about $A_V \approx 2$. This results in the typical PDR stratification of H/ H_2 and C^+/ C/ CO. The depth of this transition zone depends on the physical parameters but also on the contents of the chemical network: for example the inclusion of PAHs into the chemical balance calculations shifts the C^+ to C transition to smaller $A_{V,\mathrm{eff}}$ (e.g. Lepp & Dalgarno, 1988; Bakes & Tielens, 1998).

The chemistry calculation itself covers the destruction and formation reactions of all chemical species considered. For each included species i this results in a balance equation of the form:

$$\frac{dn_i}{dt} = \sum_j \sum_k n_j n_k R_{jki} + \sum_l n_l \zeta_{li} - n_i \left(\sum_l \zeta_{il} + \sum_l \sum_j n_j R_{ijl} \right) \quad (4)$$

The first two terms cover all formation processes while the last two terms account for all destruction reactions. R_{jki} is the reaction rate coefficient for the reaction $X_j + X_k \rightarrow X_i + ...$, ζ_{il} is the local photo-destruction rate coefficient for ionization or dissociation of species $X_i + h\nu \rightarrow X_l + ...$, either by FUV photons or by cosmic rays (CR), and ζ_{li} is the local formation rate coefficient for formation of X_i by photo-destruction of species X_l. For a stationary solution one assumes $dn_i/dt = 0$, while non-stationary models solve the differential equation 4 in time. Three major questions have to be addressed:

1. which species i should be included?
2. which reactions should be considered?
3. which reaction rate coefficients should be applied?

A general answer to question 1) cannot be given, since it depends on the field of application. In steady state one has to solve a system of M nonlinear equations, where M is the number of included species, thus the complexity of the problem scales linearly with the number of species rather than with the number of chemical reactions. Nowadays CPU time is not a major concern for the design of chemical networks. Nevertheless, in some cases a small network can give similar results as a big network. Several studies have shown that very large networks may include a surprisingly large number of 'unimportant' reactions, i.e. reactions that may be removed from the network without changing the chemical structure significantly (Markwick-Kemper, 2005; Wakelam et al., 2005a). It is more important to identify crucial species not to be omitted, i.e. species that dominate the chemical structure under certain conditions. A well known example is the importance of sulfur for the formation of atomic carbon at intermediate A_V where the charge transfer reaction $S + C^+ \rightarrow C + S^+$ constitutes an additional production channel for atomic carbon, visible in a second rise in the abundance of C (Sternberg & Dalgarno, 1995). In these benchmarking calculations, sulfur was not included in order to minimize model complexity, in spite of its importance for the PDR structure. The chemical network is a highly non-linear system of equations. Hence it is not self-evident that a unique solution exists at all, multiple solution may be possible as demonstrated e.g. by Le Bourlot et al. (1993) in certain regimes of parameter space encountered in PDRs. The numerical stability and the speed of convergence may vary significantly over different chemical networks.

Regarding question 2) a secure brute force approach would be the inclusion of all known reactions involving all chosen species, under the questionable assumption that we actually *know* all important reactions and their rate coefficients. This particularly concerns grain surface reactions and gas-grain interactions such as freeze-out and desorption. It is important not to create artificial bottlenecks in the reaction scheme by omitting important channels. The choice of reaction rate coefficients depends on factors like availability, accuracy, etc.. A number of comprehensive databases of rate coefficients is available today, e.g. NSM/OHIO (Wakelam et al., 2004, 2005b), UMIST

(Millar, Farquhar, & Willacy, 1997; Le Teuff et al., 2000), and Meudon (Le Bourlot et al., 1993), which collect the results from many different references, both theoretical and experimental.

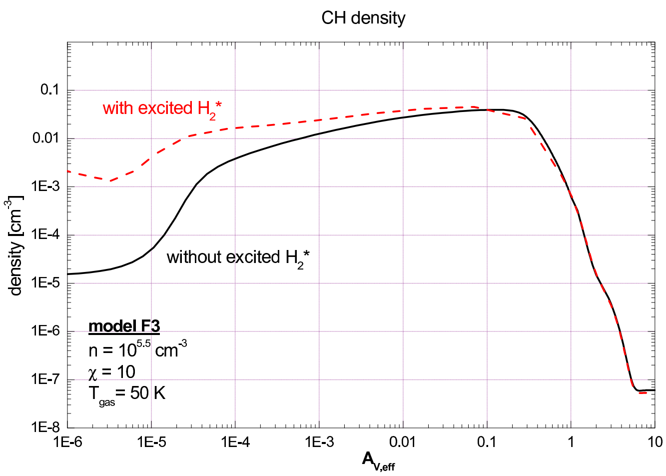

Fig. 1. Comparison between models codes with (dashed line) and without (solid line) excited molecular hydrogen, H_2^*. The abundance profile of CH is plotted for both models against $A_{V,\mathrm{eff}}$. Benchmark model F3 has a high density ($n = 10^{5.5}$ cm^{-3}) and low FUV intensity ($\chi = 10$).

An example for the importance of explicitly agreeing on the treatment of certain chemical aspects is the reaction:

$$C + H_2 \rightarrow CH + H \tag{5}$$

It has an activation energy barrier of 11700 K (Millar, Farquhar, & Willacy, 1997), effectively reducing the production of CH molecules. If we include vibrationally excited H_2^* into the chemical network and assume that reaction 5 has no activation energy barrier for reactions with H_2^* we obtain a significantly higher production rate of CH as shown in Figure 1. Of course this is a rather crude assumption, but it demonstrates the importance of explicitly agreeing on how to handle the chemical calculations in model comparisons.

Another example is the formation of C in the dark cloud part of a PDR, i.e. at values of $A_V \approx 5 - 10$. A possible formation channel for atomic carbon is the dissociation of CO by secondary UV photons, induced by cosmic rays (Le Teuff et al., 2000). In the outer parts of the PDR the impinging FUV field dominates the dissociation of CO, but for higher A_V the FUV field is effectively shielded and CR induced UV photons become important. For CO, this process depends on the level population of CO, and therefore is temperature dependent (Gredel et al., 1987). Assuming LTE, the reaction rate as given by Gredel et al. (1987) has to be corrected by a factor of $(T/300K)^{1.17}$ effectively reducing the dissociation rate for temperatures below 300 K (Le Teuff et al., 2000). In Figure 2 we plot the density profile of atomic carbon for an isothermal benchmark model with temperature $T = 50$ K. The solid line represents the model result for a temperature independent photo-rate using the average reaction rate for $T = 300$ K, compared to the results using the rate corrected for T=50 K, given by the dashed curve.

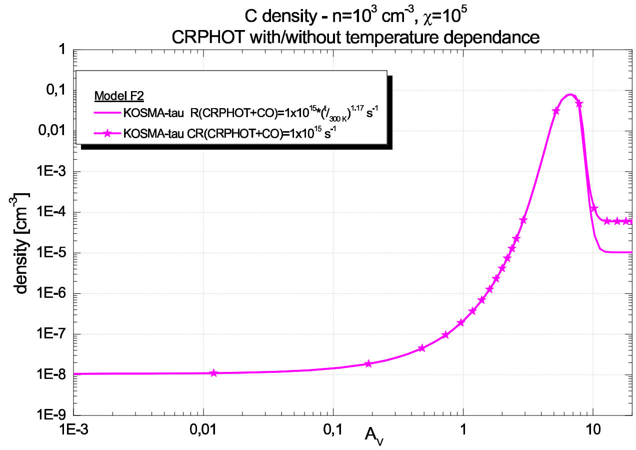

Fig. 2. The density profile of atomic carbon for the benchmark model F2 (low density, high FUV, as discussed in § 4). The solid curve results from a constant dissociation by CR induced secondary photons, the dashed curve shows the influence of a temperature dependent dissociation.

3.1.3. Heating and Cooling

To determine the local temperature in a cloud, the equilibrium between heating and cooling has to be calculated. The heating rates mainly depend on the chemical reaction rates, the grain size distribution, grain composition, and H_2 treatment, while the cooling rates are dominantly influenced by the transition rate coefficients and the dust opacity in FIR. Table 1 gives an overview of the most important heating and cooling processes. Most of them can be modelled at different levels of detail. This choice may have a major impact on the model results. One example is the influence of PAHs on the efficiency of the photoelectric heating, which results in a significantly higher temper-

Table 1. Overview over the major heating and cooling processes in PDR physics

heating	cooling
grain photoelectric heating	[CII] 158μm
PAH heating	[OI] 63, 145μm
H_2 vibrational de-excitation	[CI] 370, 610 μm
H_2 dissociation	[SiII] 35 μm
H_2 formation	CO,H_2O, OH, H_2
CR ionization	Ly α, [OI], [FeII]
gas-grain collisions	gas-grain collisions
turbulence	

ature e.g. at the surface of the model cloud. Bakes & Tielens (1994) give convenient fitting formulas for the photoelectric heating. Another important case is the vibrational de-excitation of H_2. A detailed calculation of the level population shows that for temperatures above 800 K the lowest transition may switch from heating to cooling. This imposes a significant influence on the net heating from H_2 vibrational de-excitation. When using an approximation for the heating rate it is important to account for this cooling effect (Röllig et al., 2005). The cooling of the gas by line emission depends on the atomic and molecular data as well as on the radiative transfer. A common approximation to the radiative transfer problem is by assuming escape probabilities for the cooling lines (de Jong et al., 1980; Stutzki, 1984; Störzer et al., 1996). Note that the calculation of the local escape probability by integrating $\exp(-\tau_\nu)$ over 4π gives the exact value for the escape probability of a photon at a certain location. Yet calculating the local state of excitation by using $1 - \exp(-\tau_\nu)$ integrated over 4π and thus assuming the same excitation temperature all over the cloud, is indeed an approximation. The [OI] 63μm line may also become very optically thick and can act both as heating and cooling. Under certain benchmark conditions (low density, constant temperature $T_{gas} = 50$ K) the [OI] 63μm line even showed weak masing behavior (see online data plots). Collisions between the gas particles and the dust grains also contribute to the total heating or cooling.

3.1.4. Grain Properties

Similar to the subsection § 3.1.2 on chemistry we will give a short overview of the importance of dust grains in the modeling of PDRs. Many aspects of PDR physics and chemistry are connected to dust properties. Dust acts on the energy balance of the ISM by means of photoelectric heating; it influences the radiative transfer by absorption and scattering of photons, and it acts on the chemistry of the cloud via grain surface reactions, e.g. the formation of molecular hydrogen and the depletion of other species. Often dust is split into three components: PAHs, very small grains (VSGs) and big grains (BGs).

The properties of big grains have been reviewed recently by Draine (2003, and references cited). These BGs are the main source for the dust opacity, thus determining the UV attenuation. The dust grains themselves consist of amorphous silicates and carbonaceous material and may be covered with ice mantles in the denser and colder parts of the ISM. For a detailed explanation of the composition of grains and their extinction due to scattering and absorption see Li & Draine (2002) and references therein. The first indirect evidence for the presence of VSGs in the ISM was presented by Andriesse (1978) in the case of the M17 PDR. VSGs and PAHs, with a heat content smaller than or comparable to the energy of a single photon, are subject to fluctuations in dust temperature, and are also important in the context of photoelectric heating, since their photoelectric yield is generally larger than for larger grains. Cazaux & Tielens (2004) give an overview of the present knowledge on formation of molecular hydrogen on grain surfaces and present a new model as well as comparison with laboratory results. The influence of gas depletion and grain surface reactions may be immense, but usually the inclusion of freeze-out and desorption does not affect the traditional PDR tracers. Unsuccessful attempts to detect O_2 with the SWAS and Odin (Goldsmith et al., 2000; Pagani et al., 2003; Wilson et al., 2005) satellites allow to derive upper limits for molecular oxygen which are lower than predictions of standard gas-phase chemical models. By accounting for freeze-out and surface reactions this divergence between observation and prediction may be resolved (Bergin et al., 2000; Viti et al., 2001; Roberts & Herbst, 2002) and the latest PDR models to explain H_2O and O_2 include photodesorption of H_2O ice (Dominik et al., 2005). Spaans & van Dishoeck (2001) present an alternative interpretation of the absence of O_2 in terms of clumpy PDRs.

The influence and proper treatment of electron densities together with grain ionization and recombination is still to be analyzed. Some approaches are given by Weingartner & Draine (2001). Not only the charge of dust and PAHs but also the scattering properties are still in discussion. This may heavily influence the model output. It has been shown that the inclusion of back-scattering significantly increases the total photodissociation rate, e.g of H_2, at the surface of the model cloud compared to calculations with pure forward scattering.

3.1.5. Radiative Transfer

The radiative transfer (RT) can be split into two distinct wavelength regimes: FUV and IR/FIR. These may also be labeled as 'input' and 'output'. FUV radiation due to ambient UV field and/or young massive stars in the neighborhood impinges on the PDR. The FUV photons are absorbed on their way deeper into the cloud, giving rise to the well known stratified chemical structure of PDRs. In general, reemission processes can be neglected in the FUV, considerably simplifying the radiative transfer problem. Traveling in only one direction, from the edge to the inside, the local mean FUV intensity can usually be calculated in a few iteration steps. In contrast to the FUV, the local FIR intensity is a function of the temperature and level population at all positions due to absorption and reemission of FIR photons. Thus a computation needs to iterate over all spatial grid points. A common simplifying approximation is the spatial decoupling via the escape probability approximation. This allows to substitute the intensity dependence with a dependence on the relevant optical depths, entering the escape probability. The calculation of emission line cooling then becomes primarily a problem of calculating the local excitation state of the particular cooling species. An overview of NLTE radiative transfer methods is given by van Zadelhoff et al. (2002)

3.1.6. Ionization Rate

One very important parameter for any PDR model is the cosmic ray ionization rate $\zeta_{\rm CR}$. Especially in the dark cloud part of the PDR ($A_{\rm V,eff} \gtrsim 1...10$), $\zeta_{\rm CR}$ is the dominant ionization source and thus triggers most important chemical ion-neutral reaction chains. Some of these key reactions very sensitively depend on $\zeta_{\rm CR}$, giving rise to very big differences in the resulting chemical

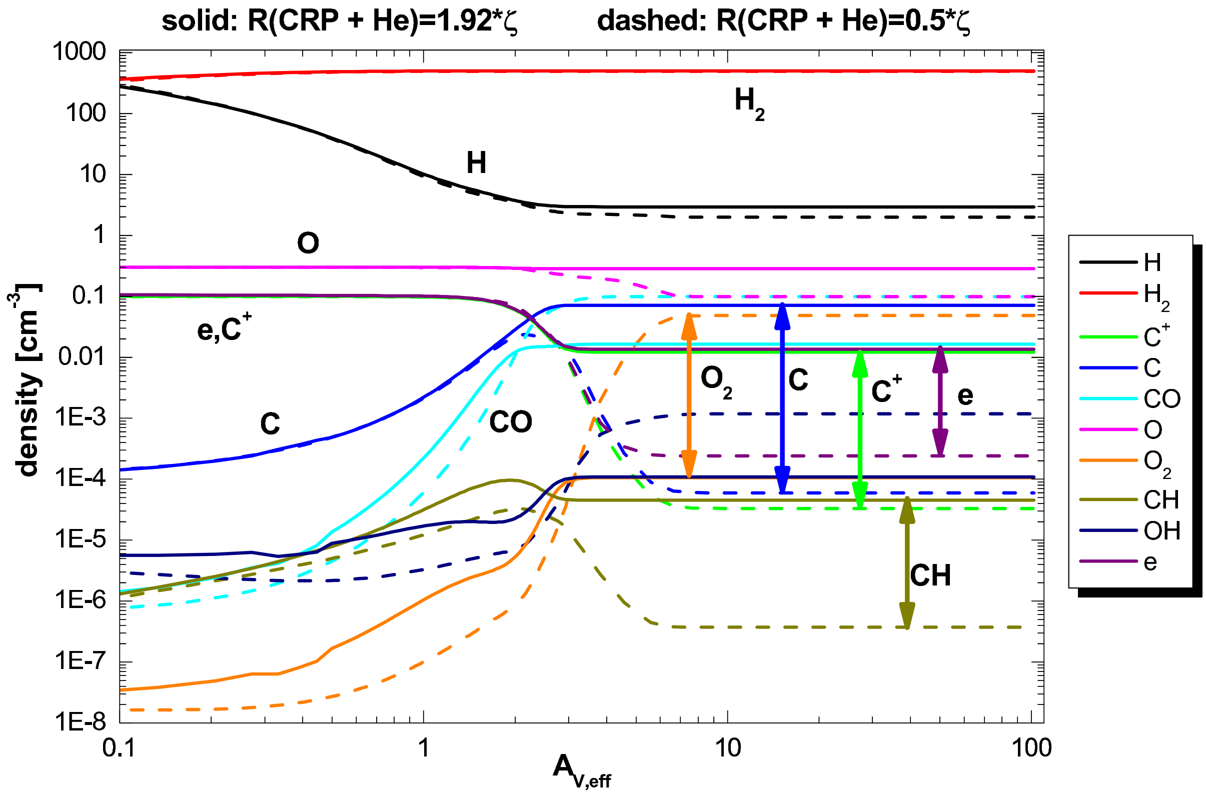

Fig. 3. Model F1 (n=10^3 cm^{-3}, χ = 10): The influence of the cosmic ray ionization rate on the chemical structure of a model cloud. The solid lines give the results for an ionization rate, enhanced by a factor 4, the dashed lines are for the lower ionization rate. The different colors denote different chemical species

structure. To demonstrate this we plotted in Fig. 3 the density profiles of two model clouds with identical input parameters (isothermal model F1) except for one single chemical reaction rate: the ionization of He by cosmic ray particles. The solid lines give the results for an ionization rate, enhanced by a factor 4, the dashed lines are for the lower ionization rate. The most prominent differences are highlighted with respectively colored arrows. The factor 4 in ζ_{CR} results in differences in density up to 4 orders of magnitude! Due to its strong influence on the chemistry of a cloud it is possible to derive the quantitative value of ζ_{CR} from the observation of certain key species (for discussion see Lintott & Rawlings (2005) and references therein). Yet the results vary by roughly a factor of 10 depending on the applied method. This uncertainty together with the fact that observations also indicate that the local CR ionization rate ζ_{CR} varies between different Galactic sources emphasizes the importance of the ionization rate for any PDR model calculation. Additionally, it demonstrates that it is difficult to simply apply PDR model results for a certain source to a different object.

4. Description of the Benchmark Models

4.1. PDR Code Characteristics

A total number of 11 model codes participated in the PDR model comparison study during and after the workshop in Leiden. Table 2 gives an overview of these codes. The codes are different in many aspects:

- finite and semi-infinite plane-parallel and spherical geometry, disk geometry
- chemistry: steady state vs. time-dependent, different chemical reaction rates, chemical network
- IR and FUV radiative transfer (effective or explicitly wavelength dependent), shielding, atomic and molecular rate coefficients
- treatment of dust and PAH
- treatment of gas heating and cooling
- range of input parameters
- model output
- numerical treatment, gridding, etc.

This manifold in physical, chemical and technical differences makes it difficult to directly compare results from the different codes. Thus we tried to standardize the computation of the benchmark model clouds as much as possible. This required all codes to reduce their complexity and sophistication, often beyond what their authors considered to be acceptable, considering detailed knowledge of some of the physical processes. However as the main goal of this study was to understand why and how these codes differ these simplifications are acceptable. Our aim was not to provide the most realistic model of real astronomical objects. The individual strengths (and weaknesses) of each PDR code are

Table 2. List of participating codes. See Appendix for short description of the individual models.

Model Name	Authors
`Aikawa`(1)	H.-H. Lee, E. Herbst, G. Pineau des Forêts, J. Le Bourlot, Y. Aikawa, N. Kuboi (Lee et al., 1996)
`Cloudy`	G. J. Ferland, P. van Hoof, N. P. Abel, G. Shaw (Ferland et al., 1998; Abel et al., 2005)
`COSTAR`	I. Kamp, F. Bertoldi, G.-J. van Zadelhoff (Kamp & Bertoldi, 2000; Kamp & van Zadelhoff, 2001)
`HTBKW`	D. Hollenbach, A.G.G.M. Tielens, M.G. Burton, M.J. Kaufman, M.G. Wolfire (Tielens & Hollenbach, 1985; Kaufman et al., 1999; Wolfire et al., 2003)
`KOSMA-`τ	H. Störzer, J. Stutzki, A. Sternberg (Störzer et al., 1996), B. Köster, M. Zielinsky, U. Leuenhagen Bensch et al. (2003),Röllig et al. (2005)
`Lee96mod`	H.-H. Lee, E. Herbst, G. Pineau des Forêts, E. Roueff, J. Le Bourlot, O. Morata (Lee et al., 1996)
`Leiden`	J. Black, E. van Dishoeck, D. Jansen and B. Jonkheid (Black & van Dishoeck, 1987; van Dishoeck & Black, 1988; Jansen et al., 1995)
`Meijerink`	R. Meijerink, M. Spaans (Meijerink & Spaans, 2005)
`Meudon`	J. Le Bourlot, E. Roueff, F. Le Petit (Le Petit et al., 2005, 2002; Le Bourlot et al., 1993)
`Sternberg`	A. Sternberg, A. Dalgarno (Sternberg & Dalgarno, 1995; Sternberg & Neufeld, 1999)
`UCL_PDR`	S. Viti, W.-F. Thi, T. Bell (Taylor et al., 1993; Papadopoulos et al., 2002)

(1) The authors could not attend the workshop.

briefly summarized in the Appendix and on the website: `http://www.ph1.uni-koeln.de/pdr-comparison.`

4.2. Benchmark Frame and Input Values

A total of 8 different model clouds were agreed upon for the benchmark comparison. The density and FUV parameter space is covered exemplary by accounting for low and high densities and FUV fields under isothermal conditions, giving 4 different model clouds. The complexity of the model calculations was reduced by setting the gas and dust temperatures to a given constant value (models F1-F4, 'F' denoting a fixed temperature), making the results independent of the solution of the local energy balance. In a second benchmark set, the thermal balance has been solved explicitly thus determining the temperature profile of the cloud (models V1-V4, 'V' denoting variable temperatures). Table 3 gives an overview of the cloud parameter of all eight benchmark clouds.

Table 3. Specification of the model clouds that were computed during the benchmark. The models F1-F4 have constant gas and dust temperatures, while V1-V4 have their temperatures calculated self consistently.

F1 T=const=50 K $n = 10^3$ cm^{-3}, $\chi = 10$	F2 T=const=50 K $n = 10^3$ cm^{-3}, $\chi = 10^5$
F3 T=const=50 K $n = 10^{5.5}$ cm^{-3}, $\chi = 10$	F4 T=const=50 K $n = 10^{5.5}$ cm^{-3}, $\chi = 10^5$
V1 T=variable $n = 10^3$ cm^{-3}, $\chi = 10$	V2 T=variable $n = 10^3$ cm^{-3}, $\chi = 10^5$
V3 T=variable $n = 10^{5.5}$ cm^{-3}, $\chi = 10$	V4 T=variable $n = 10^{5.5}$ cm^{-3}, $\chi = 10^5$

4.2.1. Benchmark Chemistry

One of the crucial steps in arriving at a useful code comparison was to agree on the use of a standardized set of chemical species and reactions to be accounted for in the benchmark calculations. For the benchmark models we only included the four most abundant elements H, He, O, and C. Additionally only the species given in Tab. 4 are included in the chemical network calculations:

Table 4. Chemical content of the benchmark calculations.

Chemical species in the models
H, H^+, H_2, H_2^+, H_3^+
O, O^+, OH^+, OH, O_2, O_2^+, H_2O, H_2O^+, H_3O^+
C, C^+, CH, CH^+, CH_2, CH_2^+, CH_3,
CH_3^+, CH_4, CH_4^+, CH_5^+, CO, CO^+,HCO^+
He, He^+, e^-

The chemical reaction rates are taken from the UMIST99 database (Le Teuff et al., 2000) together with some corrections suggested by A. Sternberg. The complete reaction rate file is available online (`http://www.ph1.uni-koeln.de/pdr-comparison`). To reduce the overall modeling complexity PAHs were neglected in the chemical network and were only considered for the photoelectric heating (photoelectric heating efficiency as given by Bakes & Tielens, 1994) in models V1-V4. Codes which calculate time-dependent chemistry used a suitably long time-scale in order to reach steady state (e.g. UCL_PDR used 100 Myr).

4.2.2. Benchmark Geometry

All model clouds are plane-parallel, semi-infinite clouds of constant total hydrogen density $n = n(\mathrm{H}) + 2\,n(\mathrm{H_2})$. Spherical codes approximated this by assuming a very large radius for the cloud. All groups were required to deliver stationary solutions, thus integrating up to $t = 10^8$ yrs for time-dependent codes.

4.2.3. Physical Specifications

As many model parameters as possible were agreed upon at the start of the benchmark calculations, to avoid initial confusion in comparing model results. To this end we set most crucial model parameters to the following values: the value for the standard UV field was taken as $\chi = 10$ and 10^5 times the Draine (1978) field. For a semi-infinite plane parallel cloud the CO dissociation rate at the cloud surface for $\chi = 10$ should equal 10^{-9} s^{-1}, using that for optically thin conditions (for which a point is exposed to the full 4π steradians as opposed to just 2π at the cloud surface) the CO dissociation rate is 2×10^{-10} s^{-1} for a unit Draine field. The cosmic ray H ionization rate is assumed to be $\zeta = 5 \times 10^{-17}$ s^{-1} and the visual extinction $A_\mathrm{V} = 6.289 \times 10^{-22} N_\mathrm{H,tot}$. If the codes do not explicitly calculate the unattenuated H_2 photo-dissociation rates (by summing over oscillator strengths etc.) we assume that the unattenuated H_2 photo-dissociation rate in a unit Draine field is equal to 5.18×10^{-11} s^{-1}, so that at the surface of a semi-infinite cloud for 10 times the Draine field the H_2 dissociation rate is 2.59×10^{-10} s^{-1}. For the dust attenuation factor in the H_2 dissociation rate we assumed $\exp(-k A_\mathrm{V})$ if not treated explicitly wavelength dependent. The value $k = 3.02$ is representative for the effective opacity in the 912-1120 Å range. We use a very simple H_2 formation rate coefficient $R = 3 \times 10^{-18} T^{1/2} = 2.121 \times^{-17}$ cm^3 s^{-1} at $T = 50$ K, assuming that every hitting atom sticks to the grain and reacts to H_2. A summary over the most important model parameters is given in Table 5.

5. Results

In the following section we give a short overview of the up to date results of the PDR model comparison. The names of the model codes are printed in typewriter font (e.g. `COSTAR`). We will refer to the two stages of the benchmarking results by pre- and post-benchmark, denoting the model results at the beginning of the comparison and at its end respectively. All pre- and post-benchmark results are posted at `http://www.ph1.uni-koeln.de/pdr-comparison`. One model from the initial 12 participating model was left out in the respective plots because the authors could not attend the workshop. In addition, the KOSMA-τ models (Röllig et al., 2005) and the models by Bensch have been merged to a single set (labeled KOSMA-τ) as they are variants on of the same basic model which do not differ for the given benchmarking parameter set, and consequently give identical results. To demonstrate the impact of the benchmark effort on the results of the participating PDR codes we plot the well known C/ C^+ / CO transition for a typical PDR environment before and after the changes identified as necessary during the benchmark in Fig. 4. The photo-dissociation of carbon monoxide is thought to be well understood for almost 20 years (van Dishoeck & Black, 1988). Nevertheless we see a significant scatter for the densities of C^+, C, and CO in the top plot of Fig. 4. The code dependent scatter in the pre-benchmark rates is significant. Most deviations could be assigned to either bugs in the pre-benchmark codes, misunderstandings, or to incorrect geometrical factors (e.g. 2π vs. 4π). This emphasizes the importance of this comparative study to establish a uniform understanding about how to calculate even these basic figures.

5.1. Models with Constant Temperature F1-F4

The benchmark models F1 to F4 were calculated with a given, fixed gas temperature of 50 K. Thus, neglecting any numerical issues, all differences in the chemical structure of the cloud are due to the different photo-rates, or non-standard chemistry. Some PDR codes used slightly different chemical networks. The code `Sternberg` uses the standard chemistry with the addition of vibrational excited hydrogen and a smaller H-H_2 formation network . The results by `Cloudy` were obtained with two different chemical setups: The pre-benchmark chemistry had the chemical network of Tielens & Hollenbach (1985). The post benchmark results use the UMIST database. `Cloudy` also used a different set of radiative recombination coefficients which were the major source for their different results (Abel et al., 2005). `Cloudy's` post-benchmark results are achieved after switching to the benchmark specifications.

In Fig. 4 we present the pre- and post-benchmark results for the main carbon bearing species C^+, C, and CO. To emphasize the pre-to-post changes we added several vertical marker lines to the plots. For C and CO they indicate the depths at which the maximum density is reached, while for C^+ they indicate the depths at which the density has dropped by a factor of 10. Dashed lines indicate pre-benchmark results, while solid lines

Table 5. Overview of the most important model parameter. All abundances are given w.r.t. total H abundance.

Model Parameters		
A_He	0.1	elemental He abundance
A_O	3×10^{-4}	elemental O abundance
A_C	1×10^{-4}	elemental C abundance
ζ_{CR}	5×10^{-17} s^{-1}	CR ionization rate
A_V	$6.289 \times 10^{-22} N_{\mathrm{H_{total}}}$	visual extinction
τ_UV	$3.02 A_v$	FUV dust attenuation
v_b	1 km s^{-1}	Doppler width
$D_{\mathrm{H_2}}$	5×10^{-18} s^{-1}	H_2 dissociation rate
R	$3 \times 10^{-18} T^{1/2}$ cm^3 s^{-1}	H_2 formation rate
$T_\mathrm{gas,fix}$	50 K	gas temperature (for F1-F4)
$T_\mathrm{dust,fix}$	20 K	dust temperature (for F1-F4)
n	$10^3, 10^{5.5}$ cm^{-3}	total density
χ	$10, 10^5$	FUV intensity w.r.t. Draine (1978) field

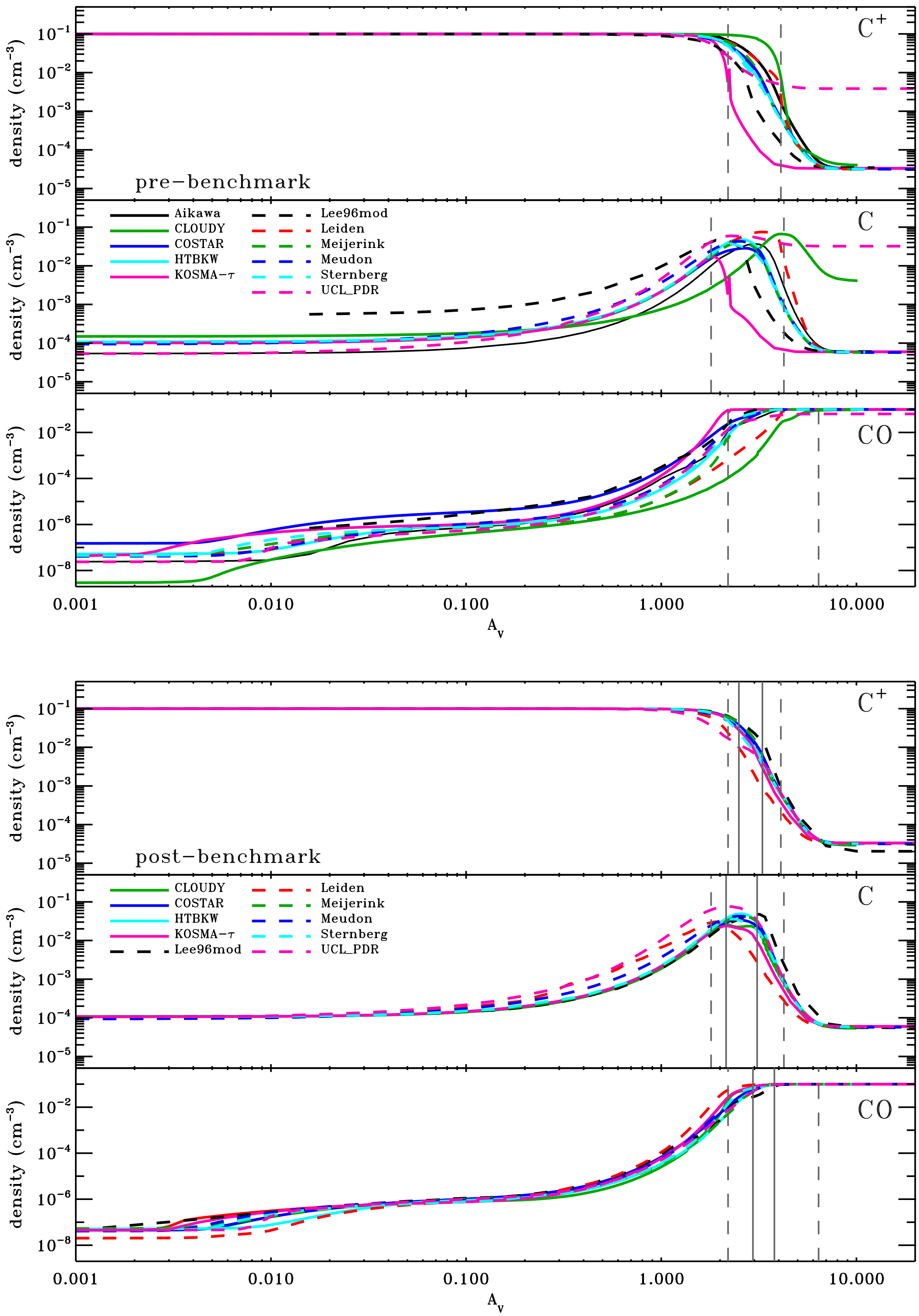

Fig. 4. Model F1 (n=10^3 cm^{-3}, χ = 10): Comparison between the density profiles of C^+ (top), C (middle), and CO (bottom) before (top) and after (bottom) the comparison study. The vertical lines indicate the code dependent scatter. For C and CO they indicate the depths at which the maximum density is reached, while for C^+ they indicate the depths at which the density dropped by a factor of 10. Dashed lines indicate pre-benchmark results, while solid lines are post-benchmark.

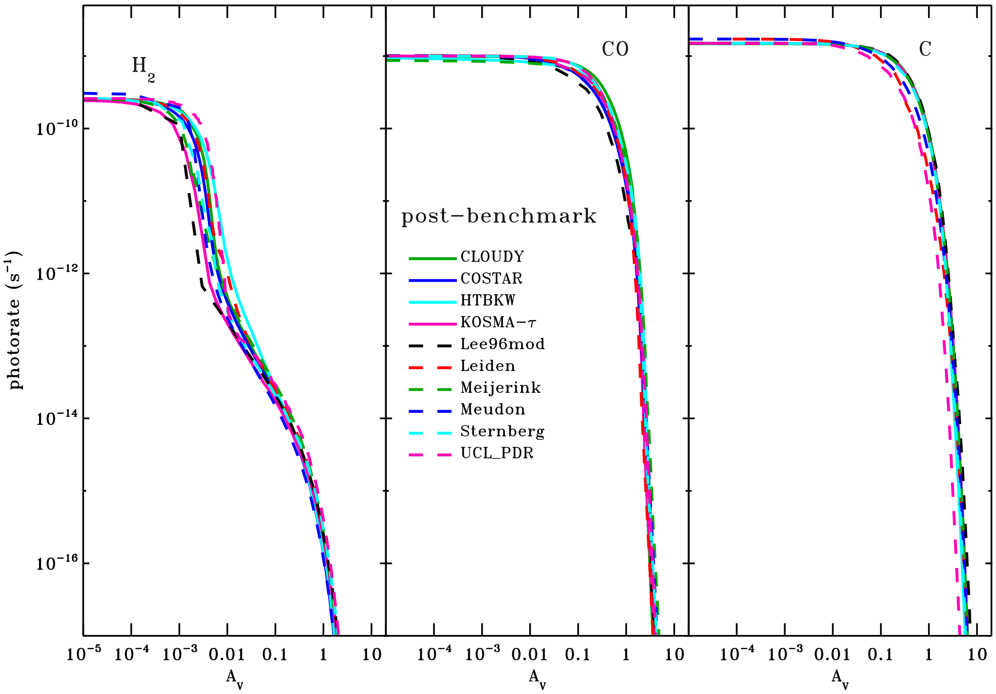

Fig. 5. Model F1 (n=10^3 cm^{-3}, χ = 10): The photo-dissociation rates of H_2 (left column), of CO (middle column) and the photo-ionization rate of C (right column) after the comparison study.

are post-benchmark. In the pre-benchmark results the code dependent scatter for these depths is $\Delta A_{\rm V,eff} \approx 2-4$ and drops to $\Delta A_{\rm V,eff} \approx 1$ in the post-benchmark results.

In the post-benchmark results, the `Leiden` and `UCL_PDR` models show a slightly different behavior. The predicted peak depth of C is a little smaller than for the other codes. The peak C density of `UCL_PDR` is also roughly 50% higher than in the other result. A comparison with the photo-ionization of C shown in Fig. 5 confirms that a slightly stronger shielding for the ionization of C is the reason for the different behavior of C and C^+. The dark cloud densities for C^+, C, and CO agree very well, except for a somewhat smaller C^+ density in the `Lee96mod` results.

In Fig. 5 we plot the photo-rates for dissociation of H_2 (left column) and CO (middle column) and for the ionization of C (right column), computed after the benchmark for model F1. Even for this simple model there are some significant differences between the models for the various rates. In the pre-benchmark results, several codes calculated different photo-rates at the edge of the model cloud, i.e. for very low values of $A_{\rm V,eff}$ (see online archive). The unshielded photo-dissociation rate of molecular hydrogen should always be the same no matter which code is being used. Even so, some codes calculated surface photo-dissociation rates between $4-5\times10^{-10}$ s^{-1} compared to the expected value of 2.59×10^{-10} s^{-1}. Most of these deviations were due to exposure to the full 4π steradians FUV field instead the correct 2π, but also due to different effects, like the FUV photon back-scattering in the `Meudon` results. The post-benchmark results (Fig. 5) show that most deviations have been corrected. The remaining offset for the `Meudon` result is due to the consideration of backscattered FUV photons, increasing the local mean FUV intensity. The pre-benchmark rates of `KOSMA-τ` was shifted toward slightly lower values of A_V because of an incorrect scaling between A_V and $A_{\rm V,eff}$ and an incorrect calculation of the angular averaged photo-rate (the model features a spherical geometry with isotropic FUV illumination). The pre- to post-benchmark changes for the photo-rates of CO and C are even more convincing (see online archive). The post-benchmark results are in very good accord except for some minor difference, e.g. `UCL_PDR's` photo-ionization rate of C showing the largest deviation from the main field.

The depth-dependence of the H_2 photo-dissociation rate is reflected in the structure of the H-H_2 transition zone. Fig. 6 shows the densities of atomic and molecular hydrogen after the benchmark. The vertical lines denote the minimum and maximum transition depths before (dashed) and after the benchmark (solid). For the pre-benchmark results the predicted transition depth ranges from 0.08 $A_{\rm V,eff}$ to 0.29 $A_{\rm V,eff}$. In the post-benchmark results this scatter is reduced by more than a factor of 3. `Sternberg` gives a slightly smaller H density in the dark cloud part. In this code, cosmic ray (CR) destruction and grain surface formation are the only reactions considered in the calculation of the H_2 density. The other codes use additional reactions. This results in a somewhat higher H density as shown in Fig. 6. This is due to:

$$H_2^+ + H_2 \rightarrow H_3^+ + H \quad (k = 2.08\times10^{-9}\,\mathrm{cm^3\,s^{-1}})$$
$$H_2 + CH_2^+ \rightarrow CH_3^+ + H \quad (k = 1.6\times10^{-9}\,\mathrm{cm^3\,s^{-1}})$$

which contribute to the total H density at high $A_{\rm V,eff}$. Even so the difference is less than a factor of two. The `Meudon` model gives a slightly smaller H_2 density at the edge of the cloud than

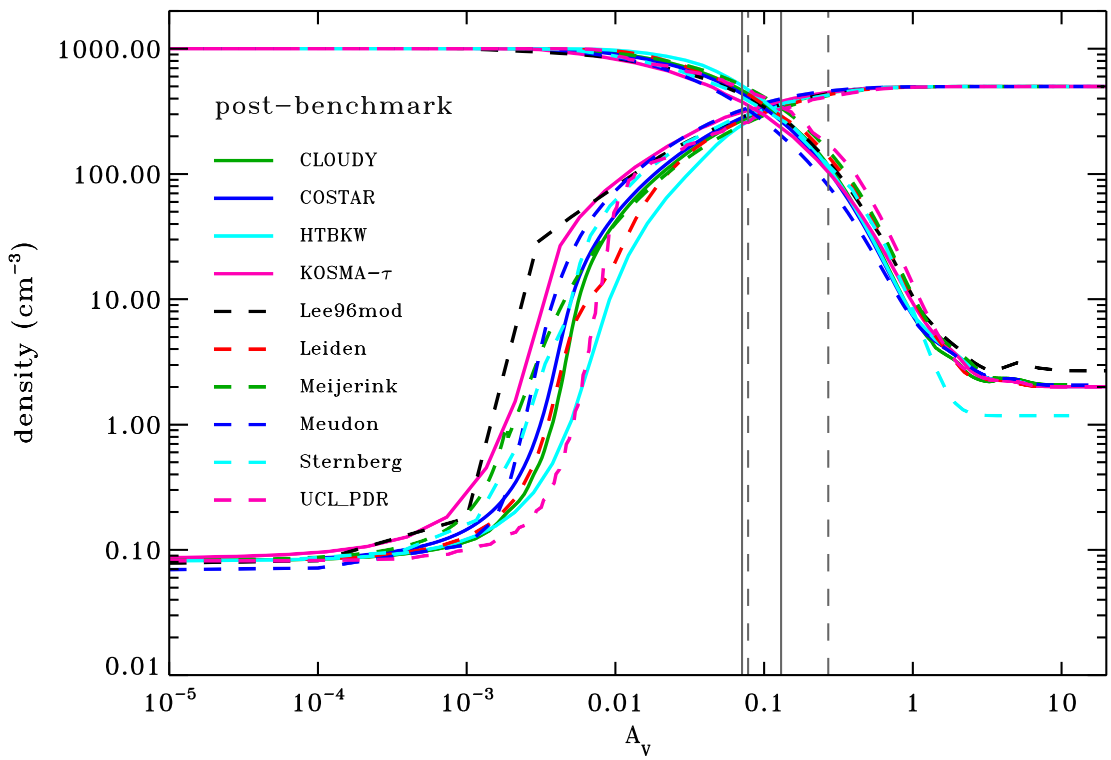

Fig. 6. Model F1 (n=10^3 cm^{-3}, χ = 10): The H-H_2 transition zone after the comparison study. Plotted is the number density of atomic and molecular hydrogen as a function of $A_{V,\mathrm{eff}}$. The vertical lines denote the range of the predicted transition depths for pre- and post-benchmark results (dashed and solid lines respectively).

the other codes. This is due to the already mentioned higher photo-dissociation rate of molecular hydrogen applied in their calculations.

The model F1 may represent a typical translucent cloud PDR, e.g., the line of sight toward HD 147889 in Ophiuchus (Liseau et al. , 1999). The low density and FUV intensity conditions help to recognize odd behavior that would be hard to noticed otherwise. This includes purely numerical issues like gridding and interpolation/extrapolation of shielding rates. This explains why the various codes still show some post-benchmark scatter. We relate differences in the predicted abundances to the corresponding rates for ionization and dissociation. Since most of the codes use the same chemical network and apply the same temperature, the major source for remaining deviations should be related to the FUV radiative transfer. To this end we present some results of benchmark model F4 featuring a density $n = 10^{5.5}$ cm^{-3} and a FUV intensity $\chi = 10^5$, in order to enhance any RT related differences and discuss them in more detail.

Fig. 7 shows the density profiles of C^+, C, and CO for the model F4. Here, the different codes are in good agreement. The largest spread is visible for the C density between $A_{V,\mathrm{eff}} \approx 3...6$. The results for C^+ and CO differ less. `Lee96mod's` results for C^+ and C show a small offset for $A_{V,\mathrm{eff}} > 6$. They produce slightly higher C abundances and lower C^+ abundances in the dark cloud part. The different codes agree very well in the predicted depth where most carbon is locked up in CO ($A_{V,\mathrm{eff}} \approx 3.5...4.5$). This range improved considerably compared to the pre-benchmark predictions of $A_{V,\mathrm{eff}} \approx 3...8$.

The results from models F1-F4 clearly demonstrate the importance of the PDR code benchmarking effort. The pre-benchmark results show a significant code-dependent scatter. Although many of these deviations could be removed during the benchmark activity, we did not achieve identical results with different codes. Many uncertainties remained even in the isothermal case, raising the need for a deeper follow up study.

5.2. Models with Variable Temperature V1-V4

In the benchmark models V1-V4 the various codes were now required to also solve the energy balance equations in order to derive the temperature structure of the model clouds. This of course introduces an additional source of variation between the codes. The chemical rate equations strongly depend on the local temperature, hence we expect a strong correlation between temperature differences and different chemical profiles of the model codes. As a consequence of a differing density profile of e.g. CO and H_2 we also expect different shielding signatures. We will restrict ourselves to just a few exemplary non-isothermal results because a full analysis of the important non-isothermal models requires more work. To study the influence of a strong FUV irradiation we show results for the

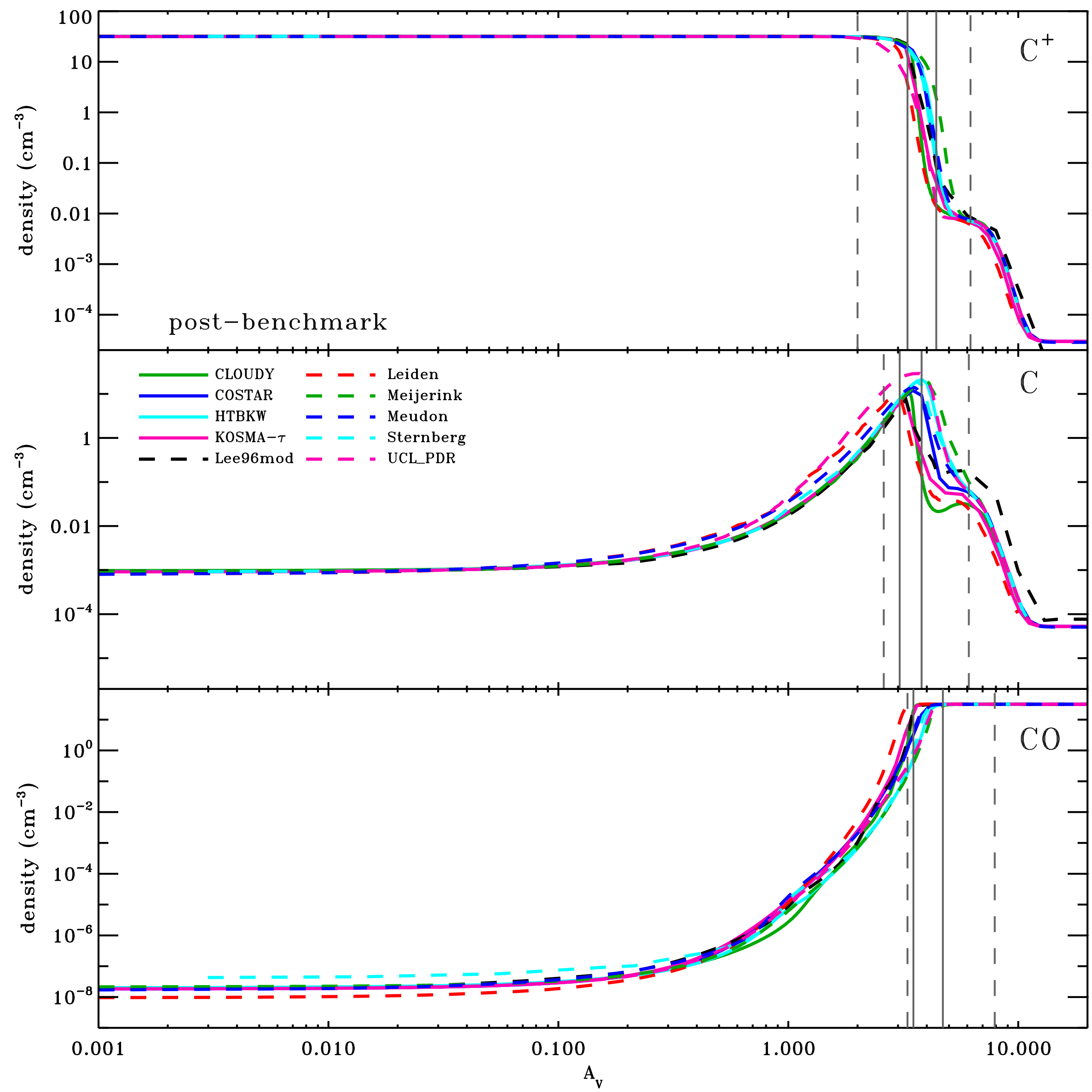

Fig. 7. Model F4 (n=$10^{5.5}$ cm^{-3}, $\chi = 10^5$): The upper panel shows the post-benchmark results for the H and H_2 densities. The lower panel shows the post-benchmark density profiles of C^+, C, and CO. The vertical gray lines in both panels indicate the pre-to-post changes.

benchmark model V2 with $n = 10^3$ cm^{-3}, and $\chi = 10^5$. The detailed treatment of the various heating and cooling processes differs significantly from code to code. The only initial benchmark requirements was to treat the photoelectric (PE) heating according to Bakes & Tielens (1994). On one hand, this turned out to be not strict enough to achieve a sufficient agreement for the gas temperatures, on the other hand it was already too strict to be easily implemented for some codes, like `Cloudy`, which calculates the PE heating self-consistently from a given dust composition. We mention this to demonstrate that there are limits to the degree of standardization. Since `Lee96mod` only accounts for constant temperatures, their model is not shown in the following plots. We only give the final, post-benchmark status.

In Fig. 8 we show the gas temperature over $A_{\mathrm{V,eff}}$. The derived temperatures at the surface vary between 1600 and

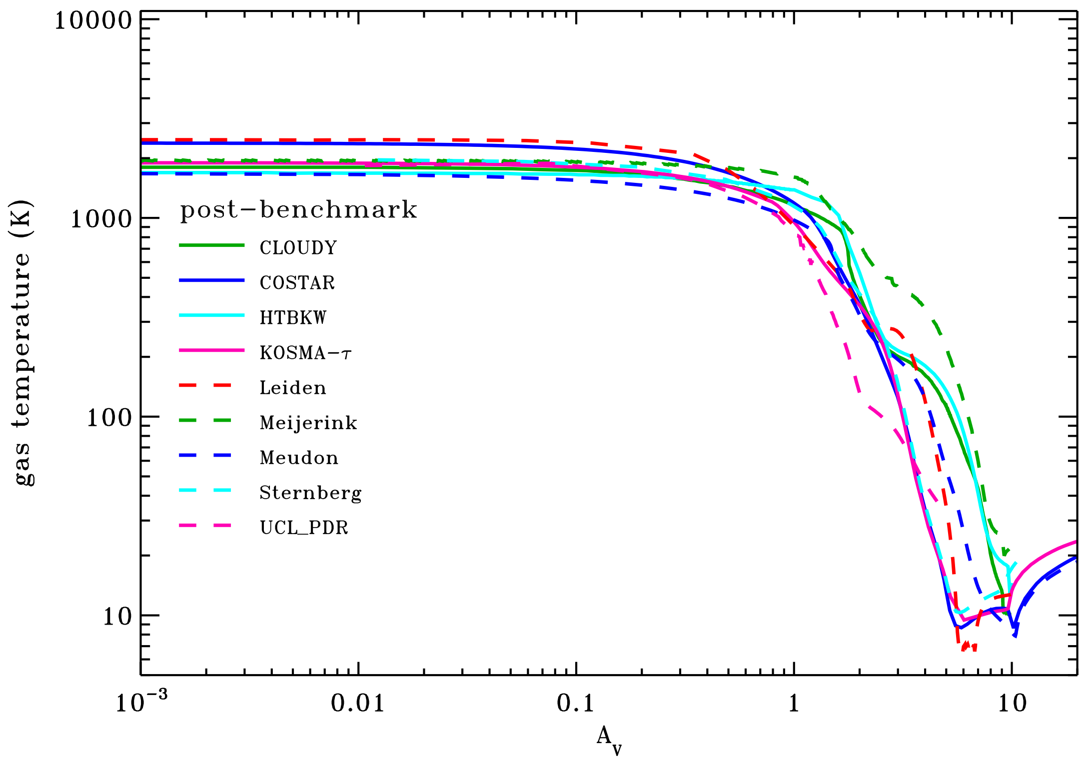

Fig. 8. Model V2 (n=10^3 cm^{-3}, χ = 10^5): The plot shows the post-benchmark results for the gas temperature.

2500 K. The heating is dominated by PE heating due to the high FUV irradiation. The main cooling is by [O I] and [C II] emission. It is interesting, that the dominant cooling line is the [O I] 63μm line, although its critical density is two orders of magnitude higher than the local density ($n_{cr} \approx 5 \times 10^5$ cm^{-3}). The highest surface temperature is calculated by `Leiden`, while `Meudon` computes the lowest temperature. The bulk of models gives surfaces temperatures near 1900 K. All models qualitatively reproduce the temperature behavior at higher values of $A_{V,eff}$ and show a minimum temperature of 10 K between $A_{V,eff} \approx 5...10$, followed by a subsequent rise in temperature. `UCL_PDR` drops earliest in T_{gas} but then shows the slowest decline compared to the other codes. The temperature minimum is not reached since they only calculated up to $A_{V,eff} = 5$. `Meijerink` computes the highest temperatures for $A_{V,eff} > 1$. They compute the strongest heating by H_2 vibrational deexcitation, which dominates the heating, and hence the temperature inside the cloud. Unfortunately, the H_2 vibrational deexcitation from different codes deviates by many orders of magnitude (see online data archive). The exact treatment of this process was not standardized and depends very much on the detailed implementation (eg. the two-level approximation from Burton, Hollenbach, & Tielens (1990) or Röllig et al. (2005) vs. solution of the full H_2 problem like in `Meudon`, `Cloudy`, and `Sternberg`). At $A_{V,eff} \approx 2...3$ we note a flattening in many models, followed by a steeper decline somewhat deeper inside the cloud. This is not the case for `HTBKW`, `KOSMA-`τ, and `Sternberg`. The reason for this behavior is the [O I] 63μm cooling, showing a steeper decline for the above codes. For very large depths, `KOSMA-`τ produces slightly higher gas temperatures. This is due to the larger dust temperature and the largest values for the central H_2 vibrational deexcitation heating. Generally, the temperatures deep inside the cloud are dominated by cosmic ray heating.

In Fig. 10 we plot the total surface brightnesses of the main fine-structure cooling lines: [C II] 158 μm, [O I] 63, and 146 μm, and [C I] 610 and 370 μm. For the KOSMA-τ model, the surface brightness averaged over the projected area of the clump is shown in Fig. 10. The surface brightness of these fine-structure line is smaller by typically a few 10%, if calculated along a pencil-beam toward the clump center. Compared with the pre-benchmark results, the spread in T_B has been decreased significantly from almost 3 orders of magnitude to a factor of 3-5 for [C II] and [O I]. `Leiden` gives the highest [O I] brightnesses. Most probably the higher intensities result from the fact that they have taken UV pumping of the fine-structure levels into account. They also compute higher local [O I] 63 μm emissivities for small values of $A_{V,eff}$. `COSTAR`, with very similar results for the density profile and comparable gas temperatures, gives much smaller emissivities. The reason for these deviations is still unclear. The model dependent spread in surface brightnesses becomes largest for the [C I] lines. `HTBKW` computes 10 times higher values for the [C I] 370μm transition than `Sternberg`. Both codes show almost

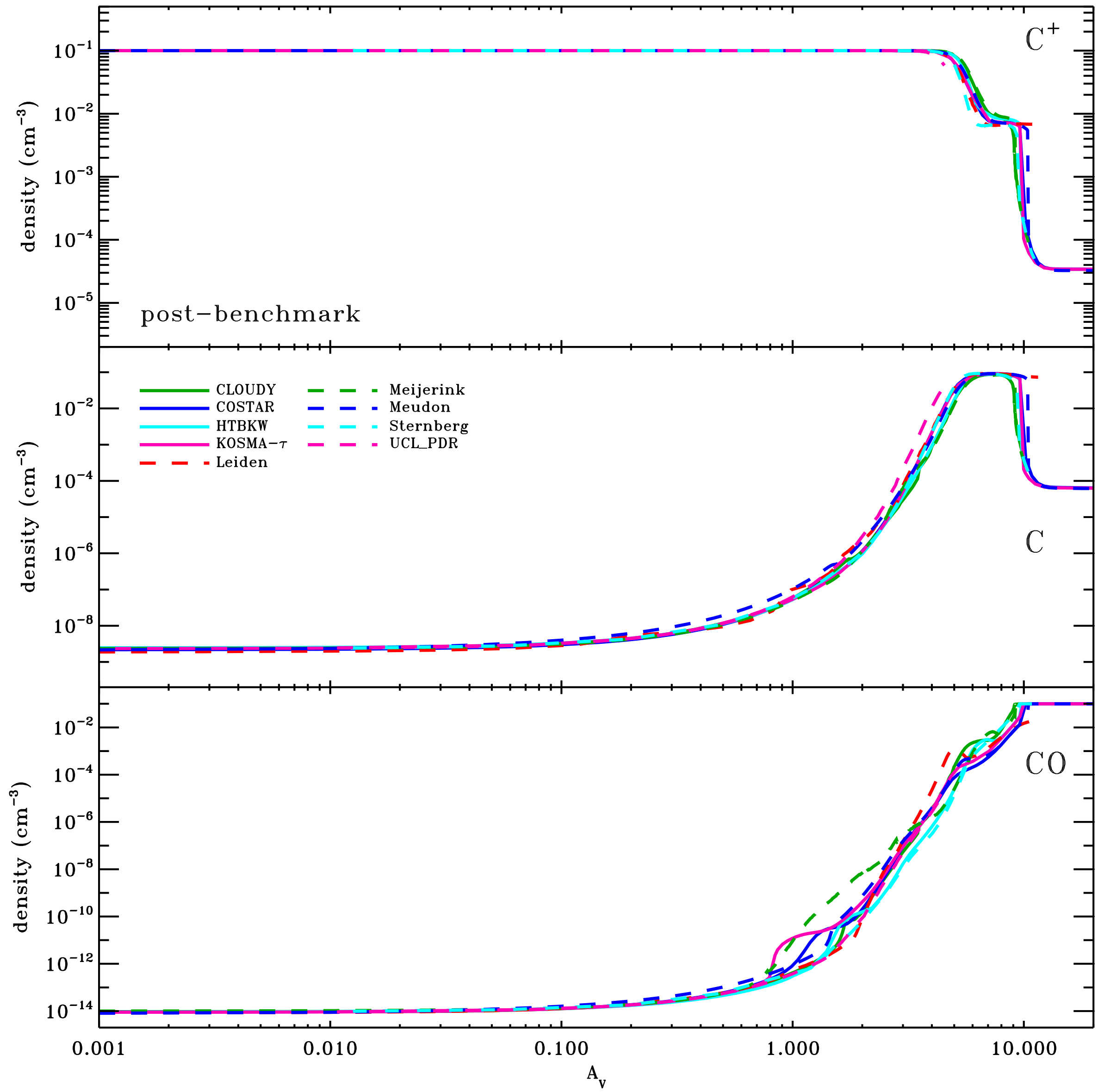

Fig. 9. Model V2 (n=10^3 cm^{-3}, $\chi = 10^5$): The post-benchmark results for the densities of C^+ (top left), the densities of C (top right), and the densities of CO (bottom left) and O and O_2 (bottom right).

identical column densities and abundance profiles of C^0, yet the local emissivities are very different between $A_{\rm V,eff} = 4...9$. `Sternberg`, together with some other codes, compute a local minimum for the cooling at $A_{\rm V,eff} \approx 6$, while the `HTBKW`, `Cloudy`, `Meijerink`, and `Meudon` models peak at the same depth. This can be explained as a pure temperature effect, since the codes showing a [C I] peak compute a significantly higher temperature at $A_{\rm V,eff} = 6$: T(`HTBKW`)=83 K, T(`Sternberg`)=10 K. These different temperatures at the C^0 abundance peak strongly influences the resulting [CI] surface brightnesses. Overall, the model-dependent surface temperatures still vary significantly. This is due to the additional nonlinearity of the radiative transfer problem, which, under certain circumstances, amplifies even small abundance/temperature differences.

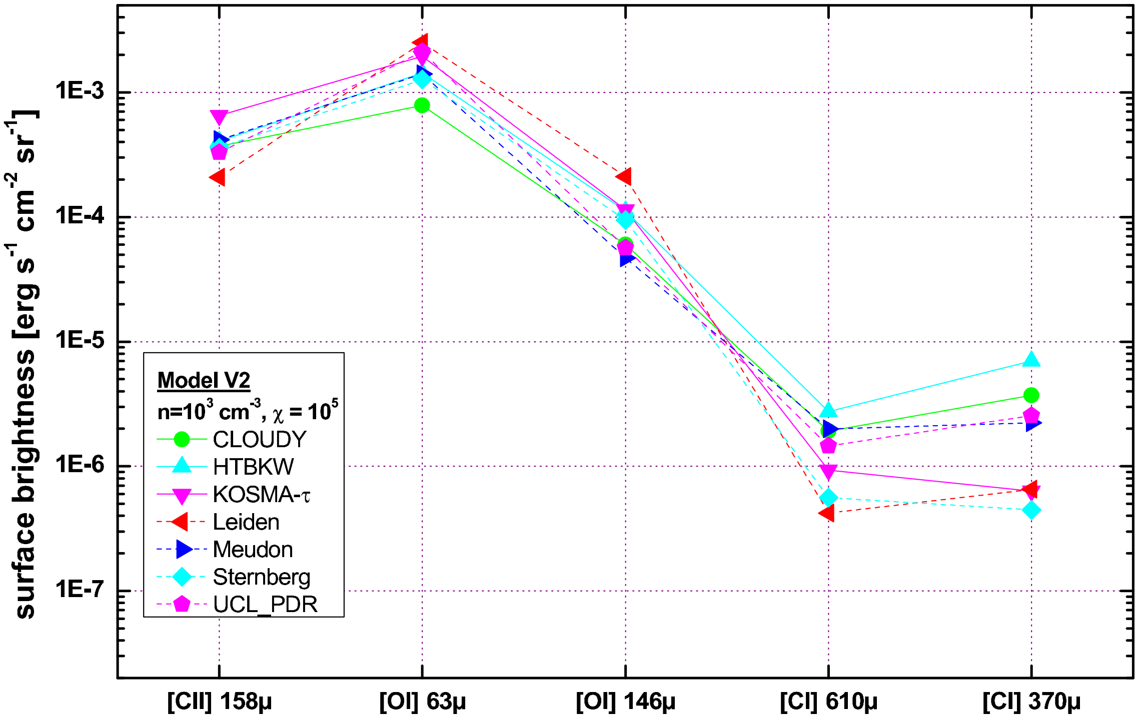

Fig. 10. Model V2 (n=10^3 cm^{-3}, $\chi = 10^5$): The plot shows the post-benchmark surface brightnesses of the main fine-structure cooling lines: [CII] 158 μm, [OI] 63, and 146 μm, and [CI] 610 and 370 μm.

5.3. Thermal balance

The temperature solutions given by the `COSTAR` and `Leiden` codes for a single input model were examined more closely. Since this was done some time before the actual benchmarking workshop, no standard chemical network or collisional rate coefficients were used; rather, each code used its own value, and the influence on the thermal balance was examined. For this test, initially only the elemental abundances, the density (3000 cm^{-3}) and the UV radiation field (χ = 30) were standardized. The initial results are shown in the top panel of Figure 11. At small optical depths the models show large discrepancies in both the gas and the dust temperature. Both codes calculate the dust temperature with a simple formula depending on χ and A_V; both codes adopting the same formula solved the differences in the dust temperature. To get agreement on the gas temperature, both the heating rates and the cooling rates had to be examinded. The photoelectric and cosmic ray heating rates were standardized, as these are the most important processes in the model under consideration.

Since at this stage the codes used different collisional excitation rates of cooling species, it was decided to calculate the populations in LTE (instead of statistical equilibrium) for the purposes of this comparison. A second point of concern was the treatment of the infrared background radiation. Initially, `Leiden` used the local dust temperature to calculate this, while `COSTAR` used the dust temperature at the edge of the PDR. It was agreed to adopt the approach of Hollenbach et al. (1991), which resembles the `COSTAR` approach. The formulae for the escape probabilities were adjusted so that the escape probability is 0.5 at the edge of the PDR and decreases with increasing optical depth (assuming a plane-parallel geometry).

The temperatures calculated by the codes after these changes were implemented can be seen in the lower panel of Figure 11. It can be seen that the g as temperatures agree well (to within a few %) in most of the PDR. The greatest discrepancy occur at A_V=2–3, where the CO abundance of `COSTAR` is much higher than that of `Leiden`. At higher optical depths the CO abundances become equal again and the temperatures are in good agreement.

6. Concluding remarks

We present the latest result in a community wide comparative study among PDR model codes. PDR models are available for almost 30 years now and are established as a common and trusted tool for the interpretation of observational data. The PDR model experts and code-developers have long recognized that the existing codes may deviate significantly in their results, so that observers have to be extremely careful when blindly using the output from one of the codes to interpret line observations. The PDR-benchmarking workshop was a first attempt to solve this problem by separating numerical and conceptional differences in the codes, and removing ordinary bugs so that the PDR codes finally turn into a reliable tool for the interpretation of observational data.

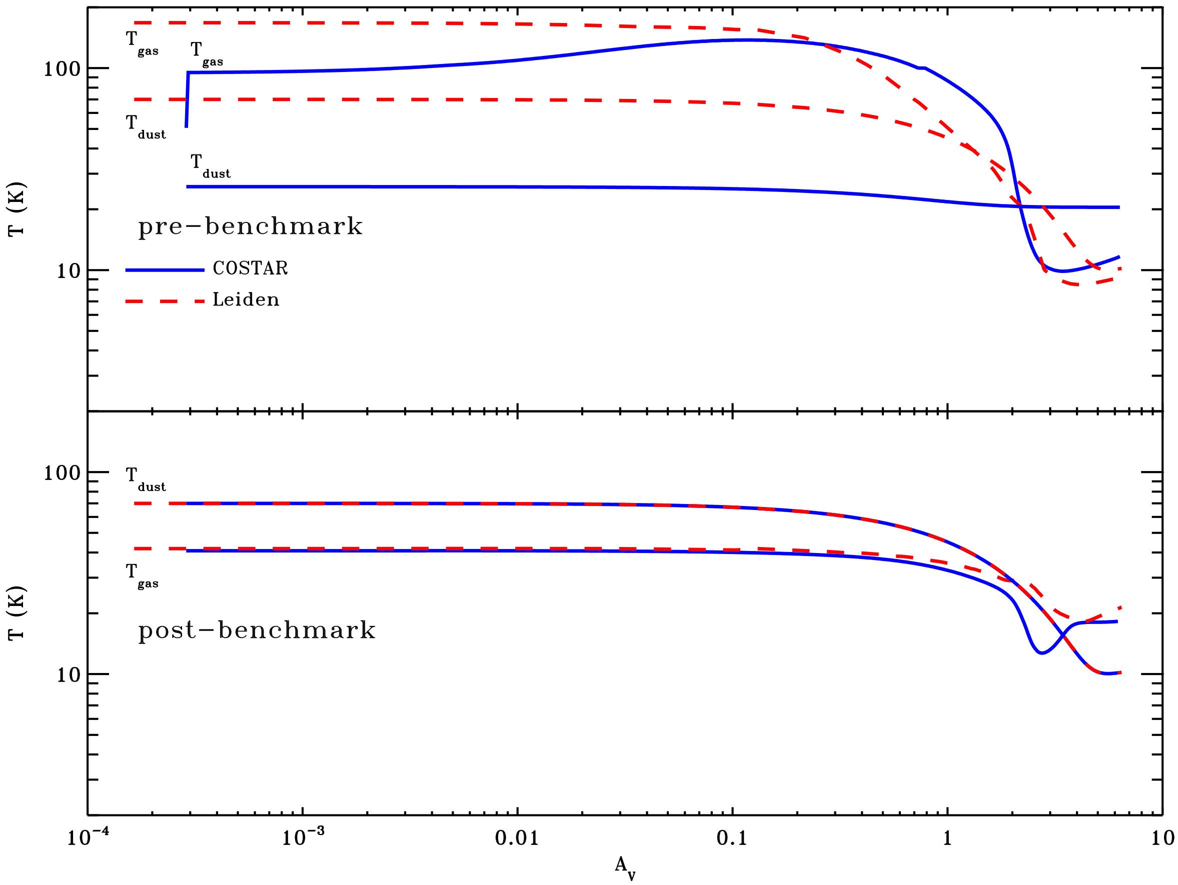

Fig. 11. The pre-benchmark (top panel) and post-benchmark (lower panel) temperature solutions of `COSTAR` and `Leiden` for a separate model to focus on the thermal balance.

Due to their complex nature it is not always straightforward to compare results from different PDR models with each other reflecting similar uncertainties with respect to the uniqueness of physical parameter sets derived by comparing observations with model predictions. Our goal was to understand the mutual differences in the different model results and to work toward a better understanding of the key processes involved in PDR modeling. The comparison has revealed the importance of an accurate treatment of various processes, which require further studies.

The workshop and the following benchmarking activities were a success regardless of many open issues. The major results of this study are:

– The collected results from all participating models represent an excellent reference for all present PDR codes and for those to be developed in the future. For the first time such a reference is easily available not only in graphical form but also as raw data. (URL: `http://www.ph1.uni-koeln.de/pdr-comparison`)
– We present an overview of the common PDR model codes and summarize their properties and field of application
– As a natural result all participating PDR codes are now better debugged, much better understood, and many differences between the results from different groups are now much clearer resulting in good guidance for further improvements.
– Many critical parameters, model properties and physical processes have been identified or better understood in the course of this study.
– We were able to increase the agreement in model prediction for all benchmark models. Uncertainties still remain,

visible e.g. in the deviating temperature profiles of model V2 (Fig. 8) or the large differences for the H_2 photo-rates and density profiles in model V4 (cf. online data archive).
– All PDR models are heavily dependent on the chemistry and micro-physics involved in PDRs. Consequently the results from PDR models are only as reliable as the description of the microphysics (rate coefficients, etc.) they are based on.

One of the lessons from this study is that observers should not take the PDR results too literally to constrain, for example, physical parameters like density and radiation field in the region they observe. The current benchmarking shows that the relative trends are consistent between codes but that there remain differences in absolute values of observables. Moreover it is not possible to simply infer how detailed differences in density or temperature translate into differences in observables. They are the result of a complex, nonlinear interplay between density, temperature, and radiative transfer. We want to emphasize again, that all participating PDR codes are much 'smarter' than required during the benchmark. Many sophisticated model features have been switched off in order to provide comparable results. Our intention was technical not physical. The presented results are not meant to model any real astronomical object and should not be applied as such to any such analysis. The current benchmarking results are not meant as our recommended or best values, but simply as a comparison test. During this study we demonstrated, that an increasing level of standardization results in a significant reduction of the model dependent scatter in PDR model predictions. It is encouraging to note the overall agreement in model results. On the other hand it is important to understand that small changes may make a big difference. We were able to identify a number of these key points, e.g. the influence of excited hydrogen, or the importance of secondary photons induced by cosmic rays.

Future work should focus on the energy balance problem, clearly evident from the sometimes significant scatter in the results for the non-isothermal models V1-V4. The heating by photoelectric emission is closely related to the electron density and to the detailed description of grain charges, grain surface recombinations and photoelectric yield. The high temperature regime also requires an enlarged set of cooling processes. As a consequence we plan to continue our benchmark effort in the future. This should include a calibration on real observational findings as well.

Acknowledgements. We thank the Lorentz Center, Leiden, for hosting the workshop and for the perfect organization, supplying a very productive environment. The workshop and this work was partly funded by the Deutsche Forschungs Gesellschaft DFG via Grant SFB494 and by a Spinoza grant from the Netherlands Organization for Scientific Research (NWO).

References

Abel, N.P., Ferland, G.J., van Hoof, P.A.M., and G.Shaw, 2005, ApJ, in print (astro-ph\0506514)
Abgrall, H., Le Bourlot, J., Pineau Des Forêts, G., Roueff, E., Flower, D.R., Heck, L., 1992, A&A, 253, 525
Andriesse, C.D., 1978, A&A, 66, 196
Arimoto N., Sofue Y., & Tsujimoto T. 1996, PASJ, 48, 275
Bakes, E. L. O. & Tielens, A. G. G. M. 1994, ApJ, 427, 822
Bakes, E. L. O.; Tielens, A. G. G. M., 1998, ApJ, 499, 258
Bensch, F., Leuenhagen, U., Stutzki, J., Shieder, R., 2003, ApJ, 591, 1913
Bergin, E.A., Melnick, G.J., Stauffer, J.R., et al., 2000, ApJ, 539, L129
Black, J. H.; Dalgarno, A., 1977, ApJS, 34, 405
Black, J. H. and van Dishoeck, E. F., 1987, ApJ, 322, 412
Boissé P. 1990, A&A, 228, 483
Bolatto, A. D., Jackson, J. M., Wilson, C. D., & Moriarty-Schieven, G. 2000, ApJ, 532, 909
Bolatto A.D., Jackson J.M., Ingalls J.G. 1999, ApJ, 513, 275
Boselli, A., Lequeux, J., & Gavazzi, G. 2002, A&A, 384, 33
Boselli, A., Gavazzi, G., Lequeux, J., Pierini, D. 2002, A&A, 385, 454
Bresolin, F. and Garnett, D. R. and Kennicutt, R. C., 2004, ApJ, 615, 228
Burke, J. R., Hollenbach, D. J., 1983, ApJ, 265, 223
Burton, M. G., Hollenbach, D. J., & Tielens, A. G. G. M. 1990, ApJ, 365, 620
Cazaux, S.; Tielens, A. G. G. M., 2004, ApJ, 604, 222
de Boisanger, C. B.; Chieze, J.-P.; Meltz, B., 1992, ApJ, 401, 182
de Jong, T., Boland, W., Dalgarno, A., 1980, A&A, 91, 68
d'Hendecourt, L., Léger, A., 1987, A&A, 180, L9
Dominik, C.; Ceccarelli, C.; Hollenbach, D.; Kaufman, M., 2005, ApJ, in print
Draine B.T. 1978, ApJS, 36, 595
Draine, B. T., 2003, ARA&A, 41, 241
Elmegreen, B. G. & Falgarone, E. 1996, ApJ, 471, 816
Ferland, G. J., Korista, K. T., Verner, D. A., Ferguson, J. W., Kingdon, J. B. and Verner, E. M., 1998, PASP, 110, 761
Flannery, B.P., Roberge, W., Rybicki, G.B., 1980, ApJ, 236, 598
Fuente, A.; Martin-Pintado, J.; Cernicharo, J.; Bachiller, R., 1993, A&A, 276, 473
Fuente, A.; Martin-Pintado, J.; Gaume, R., 1995, A&A, 442, L33
Fuente, A.; Garca-Burillo, S.; Gerin, M.; Teyssier, D.; Usero, A.; Rizzo, J. R.; de Vicente, P., 2005, ApJ, 619, L155
Gierens K.M., Stutzki J., Winnewisser G. 1992, 259, 271
Glassgold, A. E.; Langer, W. D., 1975, ApJ, 197, 347
Goldsmith, P.F., Melnick, G.J., Bergin, E.A., et al., 2000, ApJ, 539, L123
Gorti, U.; Hollenbach, D., 2002, ApJ, 573, 215
Gredel, R.; Lepp, S.; Dalgarno, A., 1987, ApJ, 323, L137
Habing, H.J., 1968, Bull. Astron. Inst. Netherlands, 19, 421
Hegmann, M.; Kegel, W. H., 1996, MNRAS, 283, 167
Hegmann, M.; Kegel, W. H., 2003, MNRAS, 342, 453
Heithausen, A., Bensch, F., Stutzki, J., Falgarone, E., & Panis, J. F. 1998, A&A, 331, L65
Henyey, L.G., and Greenstein, J.L., 1941, ApJ, 93, 70
Hogerheijde, M. R.; van der Tak, F. F. S., 2000, A&A, 362, 697
Hollenbach, D. &Salpeter, E. E. 1971, ApJ, 163, 155
Hollenbach, D. ,Werner, M. W., &Salpeter, E. E. 1971, ApJ, 163, 165

Hollenbach, D. & McKee, C. F. 1979, ApJS, 41, 555
Hollenbach D.J., Takahashi T., Tielens A.G.G.M. 1991, ApJ, 377, 192
Hollenbach D.J., Tielens A.G.G.M.,1997, ARA&A, 35, 179
Hollenbach D.J., Tielens A.G.G.M., 1999, Rev.Mod.Phys, 71,173
Howe, J. E., Jaffe, D. T., Genzel, R., & Stacey, G. J. 1991, ApJ, 373, 158
Hunter, D. A.; Kaufman, M.; Hollenbach, D. J.; Rubin, R. H.; Malhotra, S.; Dale, D. A.; Brauher, J. R.; Silbermann, N. A.; Helou, G.; Contursi, A.; Lord, S. D., 2001, ApJ, 553, 121
Israel, F. P. 1997, A&A, 328, 471
Israel, F. P.; Baas, F.; Rudy, R. J.; Skillman, E. D.; Woodward, C. E. 2003, A&A, 397, 87I
Jansen, D. J. and van Dishoeck, E. F. and Black, J. H. and Spaans, M. and Sosin, C., 1995, A&A, 302, 223
Jura, M., 1974, ApJ, 191, 375
Kamp, I. and Bertoldi, F., 2000, A&A, 353, 276
Kamp, I. and van Zadelhoff, G.-J., 2001, A&A, 373, 641
Kaufman M.J., Wolfire M.G., Hollenbach D.J., Luhman M.L. 1999, ApJ, 527, 795
Köster B., Störzer H., Stutzki J., Sternberg A. 1994, A&A, 284, 545
Kramer, C., Stutzki, J., Rohrig, R., & Corneliussen, U. 1998, A&A, 329, 249
Le Bourlot, J., Pineau Des Forêts, G., Roueff, E., & Flower, D. R. 1993, A&A, 267, 233
Le Petit, F.,, 2005, A&A, SUBMITTED
Le Petit, F., Roueff, E., Le Bourlot, J., 2002, A&A, 390, 369
Le Teuff, Y. H. and Millar, T. J. and Markwick, A. J., 2000, A&AS, 146, 157
Lee, H.-H. and Herbst, E. and Pineau des Forêts, G. and Roueff, E. and Le Bourlot, J., 1996, A&A, 311, 690
Lepp, S., Dalgarno A., 1988, ApJ, 335, 769
Lequeux, J., Le Bourlot, J., Des Forêts, G. P., Roueff, E., Boulanger, F., & Rubio, M. 1994, A&A, 292, 371
Li, A.; Draine, B. T., 2002, ApJ, 576, 762
Lintott, C.J., Rawlings, J.M.C., 2005, to be published in A&A
Liseau, R., White, G. J., Larsson, B., Sidher, S., Olofsson, G., Kaas, A., Nordh, L., Caux, E., Lorenzetti, D., Molinari, S., Nisini, B., Sibille, F., 1999, A&A, 344, 342
Madden, S. C., Poglitsch, A., Geis, N., Stacey, G. J., & Townes, C. H. 1997, ApJ, 483, 200
Madden S.C. 2000, NewAR, 44, 249
Markwick-Kemper, A.J., 2005, IAU Symposium No. 231, 2005, A.J. Markwick-Kemper ed.
Meijerink, R.; Spaans, M. , 2005, A&A, 436, 397
McKee C.F., 1989, ApJ, 345, 782
Meixner M. & Tielens, A.G.G.M. 1993, ApJ, 405, 216
Millar, T. J., Farquhar, P. R. A., & Willacy, K. 1997, A&AS, 121, 139
Mochizuki, K. and Onaka, T. and Nakagawa, T., 1998, ASP Conf. Ser., 132, 386
Nejad, L. A. M.; Wagenblast, R., 1999, A&A, 350, 204
Ossenkopf, V.; Trojan, C.; Stutzki, J., 2001, A&A, 378, 608
Pagani, L., Olofsson, A.O.H., Bergmann, P., et al., 2003, A&A, 402, L69
Pak, S., Jaffe, D. T., van Dishoeck, E. F., Johansson, L. E. B., & Booth, R. S. 1998, ApJ, 498, 735
Papadopoulos, P. P. and Thi, W.-F. and Viti, S., 2002, ApJ, 579, 270
Rawlings, J. M. C., Yates, J. A., 2001, MNRAS, 326, 1423
Röllig, M.; Hegmann, M.; Kegel, W. H., 2002, A&A, 392, 1081
Röllig, M.; Ossenkopf, V., Jeyakumar, S., Stutzki, J., Sternberg, A., 2005, A&A, submitted
Roberts, H., Herbst, E., A&A, 395, 233
Rubio, M.; Boulanger, F.; Rantakyro, F.; Contursi, A., 2004, A&A, 425, L1
Savage, C.; Ziurys, L. M., 2004, ApJ, 616, 966
Simon, R., Jackson, J. M., Clemens, D. P., Bania, T. M., & Heyer, M. H. 2001, ApJ, 551, 747
Spaans, M. 1996, A&A, 307, 271
Spaans M. & van Dishoeck E.F., 1997, A&A, 323, 953
Spaans M. & van Dishoeck E.F., 1997, ApJ, 548, L217
Stacey, G. J., Geis, N., Genzel, R., Lugten, J. B., Poglitsch, A., Sternberg, A.,& Townes, C. H., 1991, ApJ, 373, 423
Steiman-Cameron, T.Y., Haas, M.R., Tielens, A.G.G.M., Burton, M.G. 1997, ApJ, 478, 261
Sternberg A. & Dalgarno A. 1989, ApJ, 338, 197
Sternberg A. & Dalgarno A. 1995, ApJS, 99, 565
Sternberg A. & Neufeld, D. A., 1999, ApJ, 516, 371
Störzer H., Stutzki J. & Sternberg A. 1996, A&A, 310, 592
Störzer H., Zielinsky, M.; Stutzki, J.; Sternberg, A., 2000, A&A, 358, 682
Stutzki, J., 1984, Ph.D. Thesis, Universität zu Köln
Stutzki J., Stacey G.J., Genzel R., Harris A.I., Jaffe D.T. & Lugten J.B., 1988, ApJ, 332, 379
Taylor, S. D. and Hartquist, T. W. and Williams, D. A., 1993, MNRAS, 264, 929
Terzieva, R. & Herbst, E., 1998, ApJ, 501, 207
Teyssier, D.; Foss, D.; Gerin, M.; Pety, J.; Abergel, A.; Roueff, E., 2004, A&A, 417, 135
Thuan, T. X., Sauvage, M., & Madden, S. 1999, ApJ, 516, 783
Tielens A.G.G.M., Hollenbach D. 1985, ApJ, 291, 722
Trumpler, R.J., 1930, PASP, 42, 267
van Dishoeck, E.F., 1988, in Rate Coefficients in Astrochemistry, Millar T.J. and Williams D.A., (eds.) Kluwer Academic Publishers, Dordrecht, p. 49
van Dishoeck, Ewine F.; Black, John H., 1988, ApJ, 334, 771
van Zadelhoff, G.-J.; Dullemond, C. P.; van der Tak, F. F. S.; Yates, J. A.; Doty, S. D.; Ossenkopf, V.; Hogerheijde, M. R.; Juvela, M.; Wiesemeyer, H.; Schier, F. L., 2002, A&A, 395, 373
Verstrate, L., Léger, A., d'Hendecourt, L., Dutuit, O., Defourneau, D., 1990, A&A, 237, 436
Viti, S., Roueff, E., Hartquist, T.W., Pineau des Forêts, G., Williams, D.A., 2001, A&A, 370, 557
Weingartner, J. C.; Draine, B. T., 2001, ApJ, 563, 842
Wagenblast, R.; Hartquist, T. W., 1988, MNRAS, 230, 363
Wakelam, V., 2004, A&A, 413, 609
Wakelam, V., Selsis, F., Herbst, E., Caselli, P., 2005a, A&A, submitted
Wakelam, V., Herbst, E., Selsis, F., 2005, IAU Symposium No. 231, 2005b, A.J. Markwick-Kemper ed.

Walmsley, C. M.; Pineau des Forêts, G.; Flower, D. R., 1999, A&A, 342, 542
Warin, S., Benayoun, J. J., & Viala, Y. P., 1996, A&A, 308, 535
Wilson C. D. 1995, ApJ,448, L97
Wilson, C. D.; Olofsson, A. O. H.; Pagani, L.; Booth, R. S.; Frisk, U.; Hjalmarson, .; Olberg, M.; Sandqvist, Aa., 2005, A&A, 433, L5
Wolfire, M. G., Hollenbach, D., McKee, C. F., Tielens, A. G. G. M., & Bakes, E. L. O. 1995, ApJ, 443, 152
Wolfire, M. G. and McKee, C. F. and Hollenbach, D. and Tielens, A. G. G. M., 2003, ApJ, 587, 278
Zaritsky, D.; Kennicutt, R. C., Jr.; Huchra, J. P., 1994, ApJ, 420, 87
Zielinsky M., Stutzki J., Störzer H. 2000, A&A, 358